Interference effect in the scattering amplitudes for nucleon-induced two-step direct process using the sudden approximation

T. Kawano
Department of Advanced Energy Engineering Science, Kyushu University, 6-1, Kasuga-kouen, Kasuga 816-8580, Japan

S. Yoshida
Department of Physics, Tohoku University, Aoba-ku, Sendai 980-8578, Japan
(Received 21 March 2001; published 25 June 2001)

An implementation of the calculation for the two-step cross sections of the theory of Nishioka, Weidenmüller, and Yoshida is described. Cross sections that excite a $2p$-$2h$ state are expressed in a J scheme, and a Yukawa interaction is assumed for the particle-hole pair creation. The Green's function, which connects the one-step matrix element to the two-step one, is represented in r space. An interference effect among the amplitudes for the different intermediate states is examined by means of a spectroscopic amplitude. A strong interference appears for a certain configuration, and this is interpreted by a boson approximation. Microscopically calculated two-step cross sections for ^{208}Pb(p,p') reactions are averaged together with the true level density, which is based on the random matrix theory, to give a two-step cross section to the continuum energy region.

DOI: 10.1103/PhysRevC.64.024603 PACS number(s): 24.10.Eq, 24.60.Gv

I. INTRODUCTION

A quantum-mechanical approach to the preequilibrium nuclear reaction is one of the significant advances in theories for the preequilibrium process. Several quantum-mechanical theories of the preequilibrium nuclear reaction have been developed in recent years [1]. There are three well-known statistical multistep direct (MSD) theories, namely the theories of Feshbach, Kerman, and Koonin (FKK) [2], Tamura, Udagawa, and Lenske (TUL) [3], and Nishioka, Weidenmüller, and Yoshida (NWY) [4]. Those theories adopt different statistical assumptions for the multistep reactions [5], and a validation of those statistical assumptions is still under discussion [6].

The NWY theory [4] assumes that an additional particle-hole (p-h) pair creation by the incident particle is much faster than residual configuration mixing, which can be obtained by an argument of the time scale of nuclear reactions. This assumption enables us to adopt the ''sudden approximation.'' In the calculation of the two-step process with the sudden approximation, an intermediate state is always a $1p$-$1h$ state, and amplitudes for the different paths to reach the same final state interfere with each other. A statistical energy average is applied to the final state only.

In contrast with NWY, the TUL theory [3] assumes that the residual configuration mixing occurs before the new p-h pair creation. This assumption leads to the ''adiabatic approximation,'' in which a statistical energy average is applied to the intermediate state as well as the final one. Consequently, there are no interference effects among the scattering amplitudes.

These two assumptions give different expressions for the two-step cross sections. Comparisons of the calculated cross sections are, however, difficult because the NWY theory has a somewhat complicated formulation, and there are a few examples of the NWY calculations [7,8]. Koning and Akkermans [7] carried out a comparison of MSD models including FKK, TUL, and NWY. However, their implementation of the NWY calculation was simplified, so an exact calculation has not yet been done. On the other hand, TUL has been applied to analyze experimental data of nucleon-induced reactions as well as analyzing power data (Refs. [9,10], for example).

In this study, we perform calculations of the MSD two-step process with the NWY theory. To calculate a two-step process according to the NWY theory exactly, one needs to calculate distorted wave Born approximation (DWBA) matrix elements for all configurations which obey energy, angular momentum, and parity conservation. However, this is very difficult because there are a great many final $2p$-$2h$ states in a continuum energy region. Instead of that, it is more convenient to introduce a density of the final state. The two-step cross section is approximated by a product of averaged cross sections which excite various $2p$-$2h$ states and the density of the final state. A true level density [11,12] based on a random matrix model should be used for preequilibrium nuclear reaction calculations.

In Sec. II, we describe a formula of DWBA matrix elements for the two-step process in a J scheme. An interference effect among the scattering amplitudes is investigated by calculating spectroscopic amplitudes. A brief formula for the true level density in Ref. [12] is also given. Examples of the calculated two-step cross sections are shown in Sec. III.

II. MULTISTEP DIRECT REACTION WITH THE SUDDEN APPROXIMATION

A. Microscopic description of the two-step process

To describe cross sections for a MSD two-step process with the sudden approximation, an intermediate state is always a $1p$-$1h$ state, and amplitudes for the different intermediate states that lead to the same final state interfere with each other. The cross section in Fig. 1, $A+a \rightarrow C+c \rightarrow B+b$, is given by

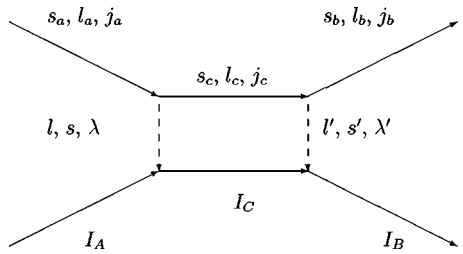

FIG. 1. Two-step process, coupling of angular momenta.

$$\left(\frac{d\sigma}{d\Omega}\right)_{\text{two step}} = \frac{2I_B+1}{(2I_A+1)(2s_a+1)} \frac{\mu_a\mu_b}{(2\pi\hbar^2)^2} \frac{k_b}{k_a} \times \sum_q \sum_{\Lambda m m_b m_a} |T_\Lambda^{m m_b m_a}(\theta)|^2, \tag{1}$$

where q is the quantum number that specifies the final $2p$-$2h$ state, I_A and I_B are the spin of the target and residual state, s_a is the intrinsic spin of the incident particle, k is the wave number, and m is the magnetic quantum number. The target, intermediate, and residual states are $0p$-$0h$, $1p$-$1h$, and $2p$-$2h$ states, respectively.

The total transferred angular momentum Λ is a vector sum of angular momentum transfers at each step, $\boldsymbol{\lambda}$ and $\boldsymbol{\lambda}'$, given by

$$\boldsymbol{\Lambda} = \boldsymbol{\lambda} + \boldsymbol{\lambda}' = \mathbf{I}_B - \mathbf{I}_A = \mathbf{j}_a - \mathbf{j}_b, \tag{2}$$

$$\boldsymbol{\lambda} = \mathbf{l} + \mathbf{s} = \mathbf{I}_C - \mathbf{I}_A = \mathbf{j}_a - \mathbf{j}_c, \tag{3}$$

and

$$\boldsymbol{\lambda}' = \mathbf{l}' + \mathbf{s}' = \mathbf{I}_B - \mathbf{I}_C = \mathbf{j}_c - \mathbf{j}_b, \tag{4}$$

where j_a, j_b, and j_c are the spin of the incoming/outgoing/intermediate particles, and $\mathbf{l}$ and $\mathbf{s}$ are the orbital angular momentum transfer and the spin transfer.

The transition matrix element $T_\Lambda^{m m_b m_a}(\theta)$ is given by [13–15]

$$T_\Lambda^{m m_b m_a}(\theta) = \sum_{I_C l s \lambda l' s' \lambda'} t(\theta) \tag{5}$$

$$\begin{aligned} t(\theta) = & \sum_{l_a j_a l_b j_b l_c j_c} i^{l_a - l_b - l - l'} (-1)^{\lambda+\lambda'-\Lambda} \hat{\Lambda}\hat{I}_C \hat{l}\hat{s}\hat{\lambda}\hat{l}'\hat{s}'\hat{\lambda}' \hat{l}_a \hat{l}_b^2 \hat{l}_c \hat{j}_b \hat{j}_c^2 \\ & \times \langle l_c l 0 0 | l_a 0 \rangle \langle l_b l' 0 0 | l_c 0 \rangle \langle l_a s_a 0 m_a | j_a m_a \rangle \langle l_b s_b - m, m_b | j_b m_b - m \rangle \\ & \times \langle j_b \Lambda m_b - m, m_a - m_b + m | j_a m_a \rangle W(j_a \lambda\, j_b \lambda'; j_c \Lambda) W(I_A \lambda\, I_B \lambda'; I_C \Lambda) \\ & \times \begin{Bmatrix} l_c & s_c & j_c \\ l & s & \lambda \\ l_a & s_a & j_a \end{Bmatrix} \begin{Bmatrix} l_b & s_b & j_b \\ l' & s' & \lambda' \\ l_c & s_c & j_c \end{Bmatrix} \sqrt{\frac{(l_b-m)!}{(l_b+m)!}} P_{l_b}^m(\theta) \\ & \times \frac{1}{k_a k_b} \int\int \chi_{l_b j_b}(k_b r_b) f_{l' s' \lambda'}(r_b) G_{l_c j_c}^{(+)}(r_b, r_a) f_{l s \lambda}(r_a) \chi_{l_a j_a}(k_a r_a) dr_b dr_a, \end{aligned} \tag{6}$$

where $\hat{j}$ stands for $\sqrt{2j+1}$, $\chi_{l_a j_a}(k_a r_a)$ and $\chi_{l_b j_b}(k_b r_b)$ are the distorted waves for the incoming/outgoing particles, $f_{ls\lambda}(r)$ is the form factor that represents the particle-hole state excitation, and $G_{l_c j_c}^{(+)}(r_b, r_a)$ is the partial-wave expanded Green's function that connects the one-step matrix element to the two-step one. The Green's function in the r-space representation [16] can be calculated as

$$G_{l_c j_c}^{(+)}(r_b, r_a) = -\frac{2\mu}{\hbar^2 k_c} \chi_{l_c j_c}(k_c r_<) \mathcal{H}_{l_c j_c}(k_c r_>), \tag{7}$$

where $\chi_{l_c j_c}(k_c r)$ is the distorted wave for the intermediate particle, $\mathcal{H}_{l_c j_c}(k_c r)$ is the out-going wave, which is an irregular solution of the Schrödinger equation, and $r_<$ ($r_>$) is the lesser (greater) of r_a and r_b.

To calculate the form factor $f_{ls\lambda}(r)$ in Eq. (6), we assume that the nucleon-nucleon interaction has the Yukawa form with the range of 1 fm. The form factor $f_{ls\lambda}(r)$ can be calculated as [17]

$$\begin{aligned} f_{ls\lambda}(r) = & \sqrt{4\pi}\sqrt{2} V_0 \hat{I}_f^{-1} (-1)^{\lambda - j_h - 1/2} i^{l_p - l_h + l} \hat{j}_h \hat{j}_p \hat{l} \hat{\lambda}^{-1} \\ & \times \langle j_p j_h 1/2, -1/2 | \lambda 0 \rangle \frac{1 + (-1)^{l_p + l_h + l}}{2} a_{ls\lambda} \\ & \times \int u_p(r') g_\lambda(r', r) u_h(r') dr', \end{aligned} \tag{8}$$

$$g_\lambda(r',r)=\frac{1}{\alpha\sqrt{rr'}}K_{\lambda+(1/2)}(\alpha r_>)I_{\lambda+(1/2)}(\alpha r'_<), \quad (9)$$

where $I_f=I_C$ for the first step and $I_f=I_B$ for the second step; l_p, l_h, j_p, and j_h are the quantum numbers of the single-particle states; $I(r)$ and $K(r)$ are the modified Bessel functions; α^{-1} is the range parameter; V_0 is the strength of effective interaction; and $a_{ls\lambda}$ is the factor defined in Ref. [17]. We assume the spin-/isospin-independent Yukawa interaction; then, $l=\lambda$, $l'=\lambda'$, and $a_{\lambda 0\lambda}=1$.

B. Spectroscopic amplitudes

For two-step (and higher) processes, there are many ways to excite a definite state, and the corresponding amplitudes interfere with each other. For the $2p$-$2h$ excitation, there are four different paths to arrive at the same final state, as shown schematically in Fig. 2. To investigate the feature of interference, we calculate the spectroscopic amplitudes. The final $2p$-$2h$ state is specified by the resultant angular momenta of two-holes I_h and two-particles I_p.

The initial state is denoted as A:$|0\rangle$, and the intermediate and the final states are

$$C:[b^\dagger_{h_1}a^\dagger_{p_1}]_{I_C M_C}|0\rangle \quad (10)$$

and

$$B:\frac{\sqrt{[1+(-1)^{I_h}\delta_{h_1h_2}][1+(-1)^{I_p}\delta_{p_1p_2}]}}{(1+\delta_{h_1h_2})(1+\delta_{p_1p_2})} \times[[b^\dagger_{h_1}b^\dagger_{h_2}]_{I_h}[a^\dagger_{p_1}a^\dagger_{p_2}]_{I_p}]_{I_BM_B}|0\rangle, \quad (11)$$

where h_1, p_1, h_2, and p_2 represent the single-particle states; $a^\dagger_i$ is the particle creation operator; and $b^\dagger_i$ is the hole creation operator. The spectroscopic amplitudes corresponding to the four paths in Fig. 2 are given by

$$A_1=\langle I_BM_B|[[b^\dagger_{h_2}a^\dagger_{p_2}]_{\lambda'}[b^\dagger_{h_1}a^\dagger_{p_1}]_{I_C}]_{I_BM_B}\rangle = P_1C_SC_N\begin{Bmatrix} j_{h_1} & j_{h_2} & I_h \\ j_{p_1} & j_{p_2} & I_p \\ I_C & \lambda' & I_B \end{Bmatrix}, \quad (12)$$

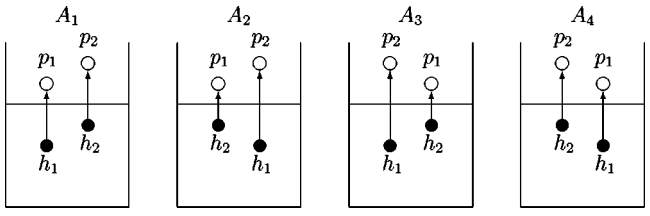

FIG. 2. Four different paths to arrive at a $2p$-$2h$ state. (1) is the basic configuration, (2) shows an exchange of the two holes, (3) shows an exchange of the two particles, and (4) shows exchanges of the two holes and two particles, respectively.

$$A_2=\langle I_BM_B|[[b^\dagger_{h_1}a^\dagger_{p_2}]_{\lambda'}[b^\dagger_{h_2}a^\dagger_{p_1}]_{I_C}]_{I_BM_B}\rangle = P_2C_SC_N\begin{Bmatrix} j_{h_1} & j_{h_2} & I_h \\ j_{p_2} & j_{p_1} & I_p \\ \lambda' & I_C & I_B \end{Bmatrix}, \quad (13)$$

$$A_3=\langle I_BM_B|[[b^\dagger_{h_2}a^\dagger_{p_1}]_{\lambda'}[b^\dagger_{h_1}a^\dagger_{p_2}]_{I_C}]_{I_BM_B}\rangle = P_3C_SC_N\begin{Bmatrix} j_{h_1} & j_{h_2} & I_h \\ j_{p_2} & j_{p_1} & I_p \\ I_C & \lambda' & I_B \end{Bmatrix}, \quad (14)$$

$$A_4=\langle I_BM_B|[[b^\dagger_{h_1}a^\dagger_{p_1}]_{\lambda'}[b^\dagger_{h_2}a^\dagger_{p_2}]_{I_C}]_{I_BM_B}\rangle = P_4C_SC_N\begin{Bmatrix} j_{h_1} & j_{h_2} & I_h \\ j_{p_1} & j_{p_2} & I_p \\ \lambda' & I_C & I_B \end{Bmatrix}, \quad (15)$$

where

$$P_1=(-1)^{I_C+\lambda'-I_B}, \quad (16)$$

$$P_2=(-1)^{j_{p_1}+j_{p_2}-I_p}, \quad (17)$$

$$P_3=(-1)^{j_{p_1}+j_{p_2}+\lambda'+I_C-I_B-I_p}, \quad (18)$$

$$P_4=-1, \quad (19)$$

and

$$C_S=\hat{I}_h\hat{I}_p\hat{\lambda}'\hat{I}_C, \quad (20)$$

$$C_N=\sqrt{[1+(-1)^{I_h}\delta_{h_1h_2}][1+(-1)^{I_p}\delta_{p_1p_2}]}. \quad (21)$$

The transition matrix element for the two-step process is a coherent sum of those paths with the corresponding spectroscopic amplitudes in Eqs. (12)–(15). When one ignores the residual interaction, the $2p$-$2h$ excitation energy is independent of I_h and I_p once the four orbits are fixed; then a cross section for a definite I_B is an incoherent sum over possible I_h and I_p. We assume that the target spin is zero, $I_A=0$; then, taking $I_C=\lambda$ and $I_B=\Lambda$, the two-step cross section in Eq. (1) becomes

$$\left(\frac{d\sigma}{d\Omega}\right)_{\text{two step}}=\frac{2\Lambda+1}{2s_a+1}\frac{\mu_a\mu_b}{(2\pi\hbar^2)^2}\frac{k_b}{k_a} \times\sum_{I_pI_h}\sum_{mm_bm_a}\left|\sum_{i=1}^{4}\sum_{\lambda\lambda'}A_it_i(\theta)\right|^2, \quad (22)$$

where $t_i(\theta)$ is given by Eq. (6).

An example of the calculated two-step cross section is shown in Fig. 3, which is an angular distribution of inelastically scattered protons on ^{208}Pb, for $E_{\text{in}}=22$ MeV, $\Lambda=2$, the excited $2p$-$2h$ state is $|1f_{7/2}0h_{9/2}(2s_{1/2})^{-1}(1d_{3/2})^{-1}\rangle$ in

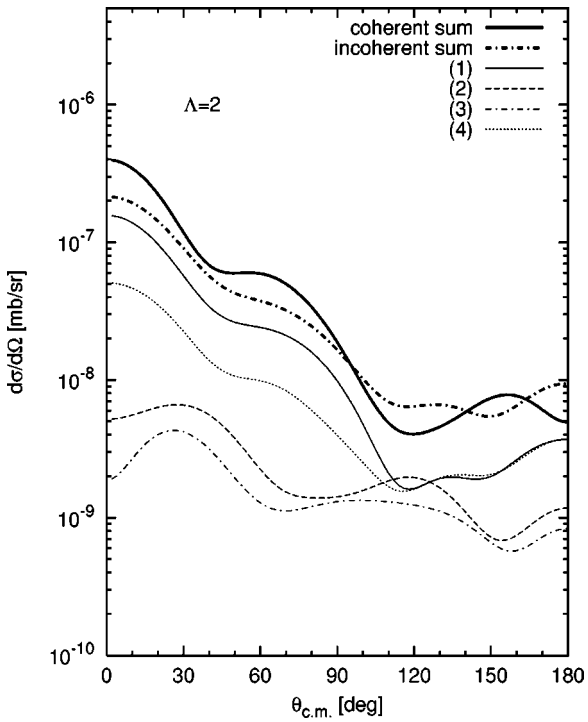

FIG. 3. Microscopic two-step cross sections for ^{208}Pb(p,p') for $E_{\rm in}=22$ MeV, $I_h=1$, $I_p=2$, and $\Lambda=2$. The $2p$-$2h$ pairs are created in the Z shell. The thin lines are the contributions of each path in Fig. 2, the thick solid line is the coherent sum of the four amplitudes, and the thick dot-dashed line is the incoherent sum.

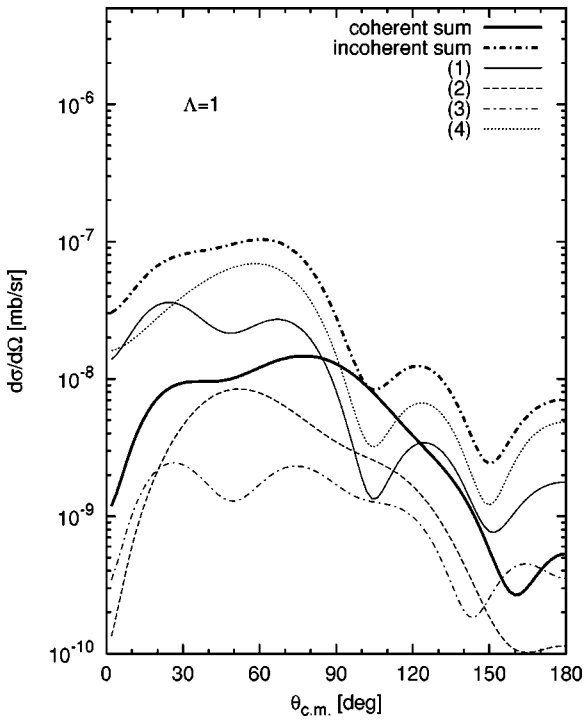

FIG. 4. Microscopic two-step cross sections for ^{208}Pb(p,p') for $E_{\rm in}=22$ MeV, $I_h=1$, $I_p=2$, and $\Lambda=1$. The $2p$-$2h$ pairs are created in the Z shell. The thin lines are the contributions of each path in Fig. 2, the thick solid line is the coherent sum of the four amplitudes, and the thick dot-dashed line is the incoherent sum.

the Z shell, and the case for $I_h=1$ and $I_p=2$. The optical potential used is the Walter-Guss potential [18] and the strength of the residual interaction V_0 is taken to be 30 MeV. The thin lines (1)–(4) are the cross sections for the different intermediate states as schematically shown in Fig. 2. The dot-dashed line is the incoherent sum of those four cross sections, while the thick solid line stands for the coherent sum of the four amplitudes. In this case, these two thick lines are in almost the same magnitude, and the interference among the scattering amplitudes is small. It is noted that we define the incoherent sum as

$$\sum_{I_pI_h}\sum_{mm_bm_a}\sum_{i=1}^{4}\left|\sum_{\lambda\lambda'}A_it_i(\theta)\right|^2, \tag{23}$$

so summations over λ and λ' are still coherent.

Figure 4 shows the same calculation as in Fig. 3 but for $\Lambda=1$. A strong interference appears in this case. The coherent sum of the four amplitudes (solid line) becomes smaller than the incoherent sum (dot-dashed line).

There are five different states specified by I_p and I_h for the $\Lambda=1$ process, namely $(I_h,I_p)=(1,1)$, (1,2), (2,1), (2,2), and (2,3). For $\Lambda=2$, there are seven states. The cross sections for those states are incoherently summed to give cross sections for the final state I_B. Those are shown in Figs. 5 and 6. A cross section for the case of $(I_h,I_p)=(2,1)$ is not shown in Fig. 5, because the spectroscopic amplitudes for $(I_h,I_p)=(1,1)$ and (2,1) of $\Lambda=2$ are the same and the cross sections for those processes become identical. This numerical equality in the spectroscopic amplitudes just happened to this case.

If the intermediate state C is a one-boson state and the final state B is a two-boson state, the spectroscopic amplitudes in the case of $p_1\neq p_2$ and $h_1\neq h_2$ become

$$A_1=1, \tag{24}$$

$$A_2=A_3=0, \tag{25}$$

$$A_4=(-1)^{I_C+\lambda'-I_B}. \tag{26}$$

We refer to this as a boson approximation. With this approximation, the complicated spectroscopic amplitudes in Eqs. (12)–(15) become just ±1 as in Eqs. (24) and (26). This helps us to understand the interference effect.

The final state in Figs. 5 and 6 is $|[[1f_{7/2}(2s_{1/2})^{-1}]_{I_1}[0h_{9/2}(1d_{3/2})^{-1}]_{I_2}]_{I_BM_B}\rangle$, where I_1 and I_2 are the quantum numbers which specify the final two-boson state. Since we assumed $I_A=0$, then $I_1=I_C=\lambda$, $I_2=\lambda'$, and $I_B=\Lambda$. From Eqs. (24) and (26), an exchange of two bosons coherently contributes to the scattering amplitudes.

The calculated cross sections with the boson approximation are shown in Figs. 5 and 6 by the thick dot-dashed lines. In the case of $\Lambda=2$ in Fig. 5, $(I_1,I_2)=(3,3)$ and (3,5) are possible; then the cross sections for those states are incoherently summed, and this can be compared with the cross sec-

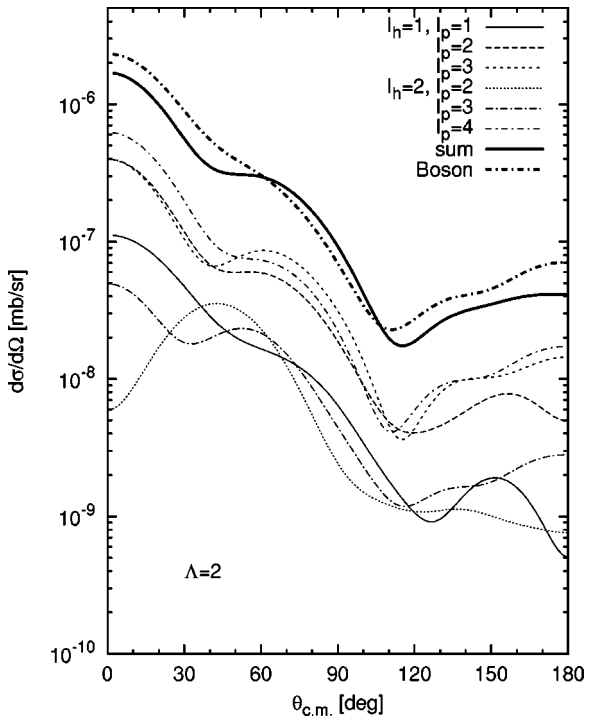

FIG. 5. Cross sections for all possible I_h and I_p numbers are shown by the thin lines, the thick solid line shows the sum of them, and the dot-dashed line is obtained with the boson approximation. The reaction is the same as in Fig. 3.

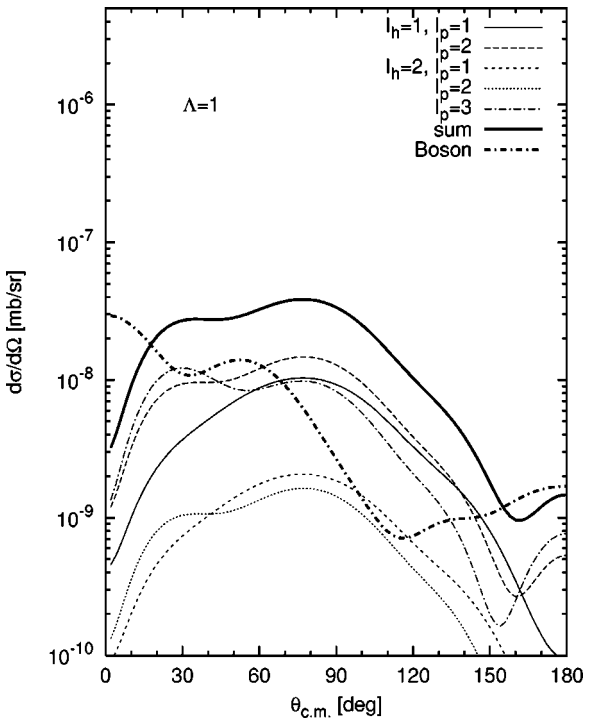

FIG. 6. Cross sections for all possible I_h and I_p numbers are shown by the thin lines, the thick solid line shows the sum of them, and the dot-dashed line is obtained with the boson approximation. The reaction is the same as in Fig. 4.

tion summed over I_p and I_h. The spectroscopic amplitudes for this case are $A_1=A_4=1$, and the boson approximation gives a good estimate. In Fig. 6, $(I_1,I_2)=(3,3)$ is allowed. The strong interference effect appeared again because of $A_1=1$ and $A_4=-1$. Therefore, the feature of the interference for these two cases can be interpreted by the boson approximation.

C. True level density

The Hamiltonian of our nucleus is assumed to consist of the single-particle Hamiltonian h and the residual interaction V, $H=h+V$. The eigenfunction and eigenvalue of the total Hamiltonian satisfy $(H-E_a)|a\rangle=0$, where a indicates the quantum numbers. For the single-particle Hamiltonian $(h-\epsilon_{m\mu})|m\mu\rangle=0$, where m represents the exciton number or $2n$ characterizing the class, and μ represents the other quantum numbers. We use the M representation to μ. The unperturbed state density $\rho_m^{(0)}(E,M)$ is given by

$$\rho_m^{(0)}(E,M)=\sum_{\mu}\ \delta(E-\epsilon_{m\mu}), \tag{27}$$

where $M=\Sigma_\alpha m_\alpha$, and m_α is the z component of the total angular momentum of the single-particle orbit α. Parity is not explicitly shown here. One can express Eq. (27) in a J scheme with the following well-known relation:

$$\rho_m^{(0)J}(E)=\rho_m^{(0)}(E,M=J)-\rho_m^{(0)}(E,M=J+1). \tag{28}$$

As the interaction V is diagonal with respect to M, we consider the subspace with a definite value of M. The matrix elements of the residual interactions V are assumed to form a Gaussian orthogonal ensemble (GOE) characterized by

$$\overline{V_{m\mu,n\nu}}=0, \tag{29}$$

$$\overline{V_{m\mu,n\nu}V_{m'\mu',n'\nu'}}=\mathcal{M}_{mn}(\delta_{mm'}\delta_{nn'}\delta_{\mu\mu'}\delta_{\nu\nu'}+\delta_{mn'}\delta_{nm'}\delta_{\mu\nu'}\delta_{\nu\mu'}), \tag{30}$$

where the bar indicates the ensemble average and $\mathcal{M}_{mn}$ is the second moment. The J-scheme second moments can be obtained by using the following relation:

$$\sum_{\mu\nu}\ (V_{m\mu,n\nu})^2_M-\sum_{\mu\nu}\ (V_{m\mu,n\nu})^2_{M+1}$$

$$=\sum_{\mu\nu}\ (V_{m\mu,n\nu})^2_{M=J}=\mathcal{M}_{mn}(J)N_m(J)N_n(J), \tag{31}$$

where

$$N_m(J)=\int\ \rho_m^{(0)J}(E)dE. \tag{32}$$

The true level density is calculated as

$$\rho^J_{m\mu}(E)=\overline{\sum_a |\langle a|m\mu\rangle|^2\delta(E-E_a)}$$
$$=-\frac{1}{\pi}\mathrm{Im}\overline{\langle m\mu|\frac{1}{E^+-H}|m\mu\rangle}$$
$$=-\frac{1}{\pi}\mathrm{Im}\langle m\mu|\frac{1}{E^+-h-\sigma^J_m(E)}|m\mu\rangle$$
$$=-\frac{1}{\pi}\mathrm{Im}\frac{1}{E^+-\epsilon_{m\mu}-\sigma^J_m(E)}, \quad (33)$$

and the exciton state density is given by

$$\rho^J_m(E)=\sum_\mu \rho^J_{m\mu}(E)=-\sum_\mu \frac{1}{\pi}\mathrm{Im}\frac{1}{E^+-\epsilon_{m\mu}-\sigma^J_m(E)}$$
$$=-\frac{1}{\pi}\int \rho^{(0)J}_m(\epsilon)\mathrm{Im}\frac{1}{E^+-\epsilon-\sigma^J_m(E)}d\epsilon. \quad (34)$$

In performing the ensemble average, we introduce the Hubbard-Stratonovich transformation and express the generating function in a form of integral over the variable σ whose saddle-point value appears in the level density formula. This value is obtained by solving the following equation:

$$\sigma^J_m(E)=\sum_n \mathcal{M}_{mn}(J)\sum_\mu \frac{1}{E-\epsilon_{m\mu}-\sigma^J_n(E)}$$
$$=\sum_n \mathcal{M}_{mn}(J)\int \rho^{(0)J}_n(\epsilon)\frac{1}{E-\epsilon-\sigma^J_n(E)}d\epsilon. \quad (35)$$

The total exciton state density is defined as

$$\rho_m(E)=\sum_J (2J+1)\rho^J_m(E), \quad (36)$$

where $\rho^J_m(E)$ is given by Eq. (34).

It is noted that the ''true'' level density obtained here (with approximation) depends on the unperturbed energy of the state $m\mu$ and σ_m, and not its structure.

The unperturbed level density $\rho^{(0)}_m(E)$ is shown in Fig. 7, which is obtained by summing over J^π with a factor of $2J+1$ as in Eq. (36). The Woods-Saxon potential was used to generate single-particle states. The binding energies of the states are the same as those employed in Ref. [19]. For deeply bound states, we used the spherical Nilsson model with the parameters of Bengtsson and Ragnarsson [20].

The calculated partial level densities in Eq. (36) for ^{208}Pb are shown by thick lines in Fig. 8 as functions of excitation energy. The Yukawa-type residual interaction with the range of 1 fm and the strength of 30 MeV was assumed. State densities calculated with a model of Běták and Dobeš [21] are also shown in this figure by thin curves. This model is based on the equidistant spacing model [22,23], and it is often adopted in precompound calculations. The single-particle state density was calculated by $g=6a/\pi^2$, where a is the level density parameter taken to be 15.36 MeV^{-1} [24].

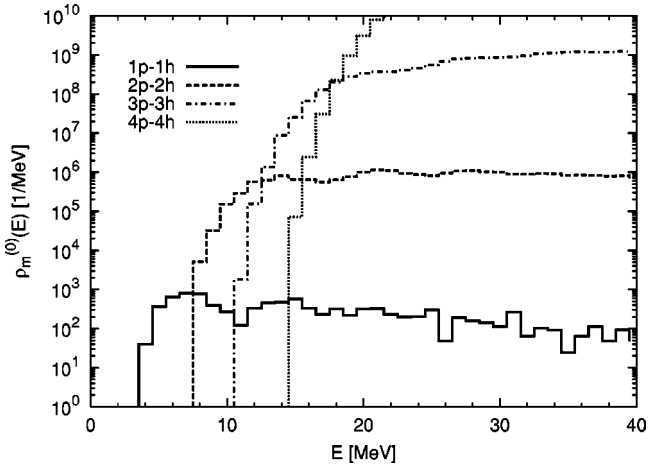

FIG. 7. Unperturbed level densities of ^{208}Pb for $m=2$–8.

It is found that the saddle-point values $\sigma^J_m(E)$ depend very weakly on J^π, so $\sigma_m(E)$ ($m=2$ and 4) averaged over J^π are shown in Fig. 9. Each particle-hole state shifts and spreads due to residual interaction, and σ_m represents the energy shift (real part) and spreading width (imaginary part). Figure 9 shows that p-h states at low excitation energies shift to lower energy and the energy shift is about -1.5 MeV, while the p-h energy increases at high excitation energies. At low excitation energies, all p-h states shift to lower energy since $\mathrm{Re}(\sigma_m)<0$, and this results in a significant enhancement of the state density near threshold energies. On the other hand, one cannot see clearly the effect of the residual interaction above that, because the exciton state densities become insensitive to the excitation energy.

III. TWO-STEP CROSS SECTIONS AND DISCUSSIONS

To calculate a double-differential cross section to the continuum energy region, one has to calculate Eq. (22) for all

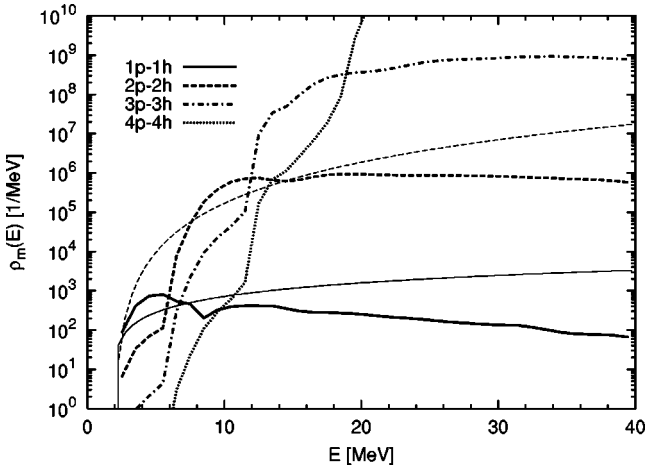

FIG. 8. Calculated partial level densities of ^{208}Pb for $m=2$–8. The thin lines are calculated with the equidistant spacing model of Běták and Dobeš for $m=2$ and 4.

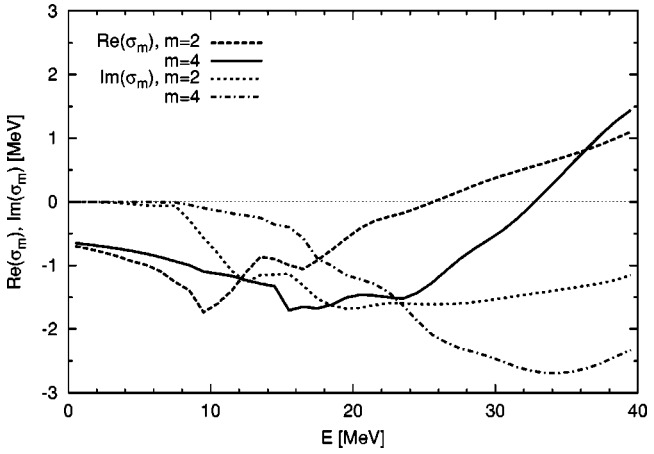

FIG. 9. Saddle-point values $\sigma_m(E)$ of ^{208}Pb for $m=2$ and 4.

final states that satisfy the energy, spin, and parity conservation in the process, and whose cross sections are multiplied by the true level density. This can be written as

$$\left(\frac{d^2\sigma}{dEd\Omega}\right)_{\text{two step}} = \sum_B (2I_B+1)\rho_m^{I_B}(E_x)\left(\frac{d\sigma}{d\Omega}\right)_B, \quad (37)$$

where B is the final state, $(d\sigma/d\Omega)_B$ is the two-step cross section in Eq. (22) but divided by $2\Lambda+1$, and $m=4$. The true level density $\rho_m^{I_B}$ for B is given by

$$\rho_m^{I_B}(E_x) = -\frac{1}{\pi}\text{Im}\frac{1}{E_x-\epsilon_B-\sigma_m^{I_B}(E_x)}, \quad (38)$$

where ϵ_B is the p-h energy for the final state B. Such calculations are, however, very difficult because there exists a large number of final states. Therefore, we approximate it by a Gaussian energy-averaged cross section [25,26] for arbitrary sampled $2p$-$2h$ states, and the averaged cross sections are multiplied by the exciton state density as

$$\left(\frac{d^2\sigma}{dEd\Omega}\right)_{\text{two step}} = \sum_\Lambda (2\Lambda+1)\rho_m^\Lambda(E_x)\overline{\left(\frac{d\sigma}{d\Omega}\right)}_\Lambda, \quad (39)$$

where the density $\rho_m^\Lambda(E_x)$ is given by Eq. (34), which is independent of the p-h energies ϵ_B for final states, and $\overline{(d\sigma/d\Omega)}_\Lambda$ is the energy-averaged value of $(d\sigma/d\Omega)_B$.

Figure 10 shows various cross sections (thin lines) for the ^{208}Pb(p,p') reaction, $\Lambda=2$ and 3, $E_{\text{in}}=30$ MeV, and $E_{\text{out}}=15$ MeV. The strength of $V_0=30$ MeV was employed. More than a hundred states for each Λ value within the energy of $E_x\pm 2$ MeV were sampled. This energy-averaging width is comparable to the energy shift due to residual interaction. The thick dotted lines in Fig. 10 are the averaged cross sections multiplied by the true level density. Such calculations were carried out for $\Lambda=0$ to 9, and those cross sections were summed to give a total two-step cross section.

The averaged cross sections for various Λ values are shown in Fig. 11 by the thin lines. These cross sections, except for $\Lambda=0$, show smooth, structureless, forward-peaked angular distributions as usually observed experimentally. For the case of $\Lambda=0$, an oscillatory angular distribution still persists because the sampling number is insufficient, and the number of possible transitions is not so large.

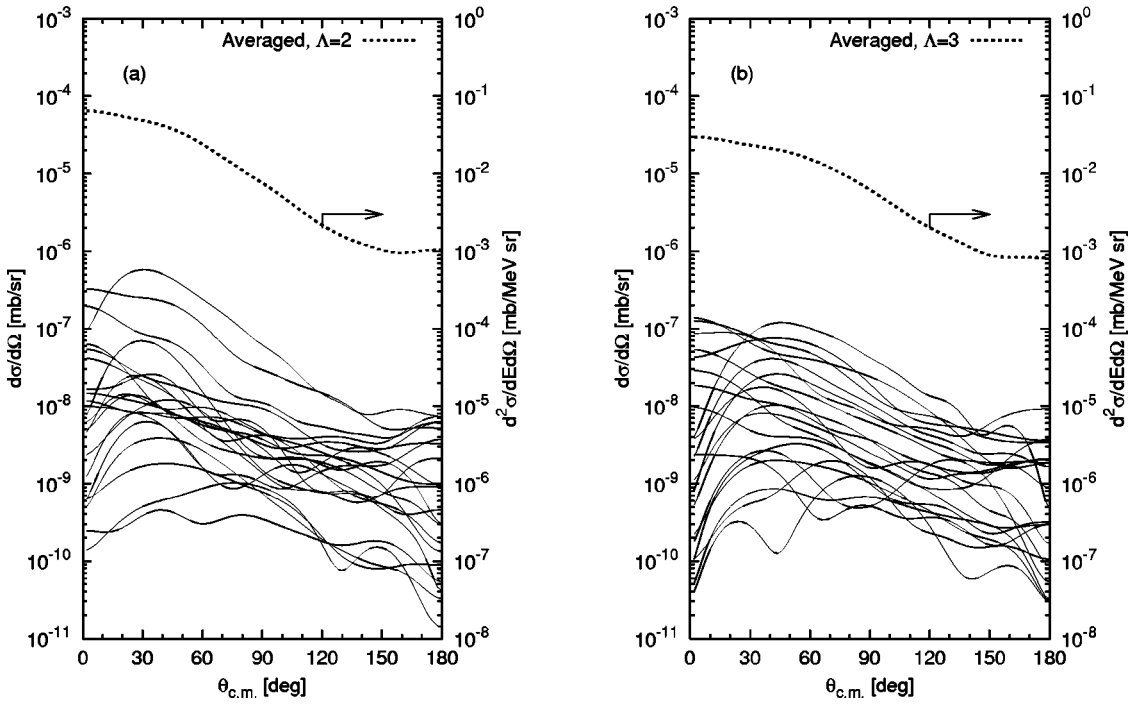

FIG. 10. Averaged microscopic two-step cross sections for ^{208}Pb(p,p') for $E_{\text{in}}=30$ MeV and $E_{\text{out}}=15$ MeV. The $\Lambda=2$ and 3 cases are shown in the left and right drawings, respectively. The thick dotted lines are the averaged values multiplied by the state density (on the right axis) and the thin lines are examples of some typical microscopic cross sections (on the left axis).

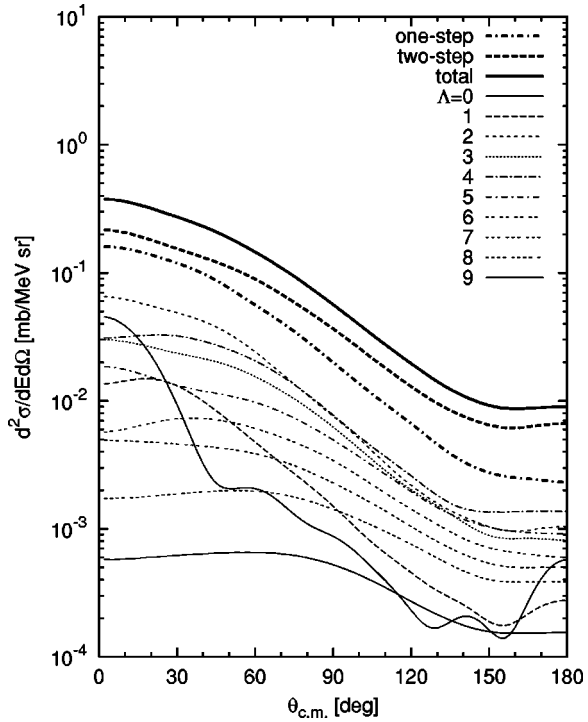

FIG. 11. Double-differential cross sections of the two-step process, ^{208}Pb(p,p') reaction at $E_{\rm in}=30$ MeV and $E_{\rm out}=15$ MeV. Contributions of the various Λ values, and the sum of them.

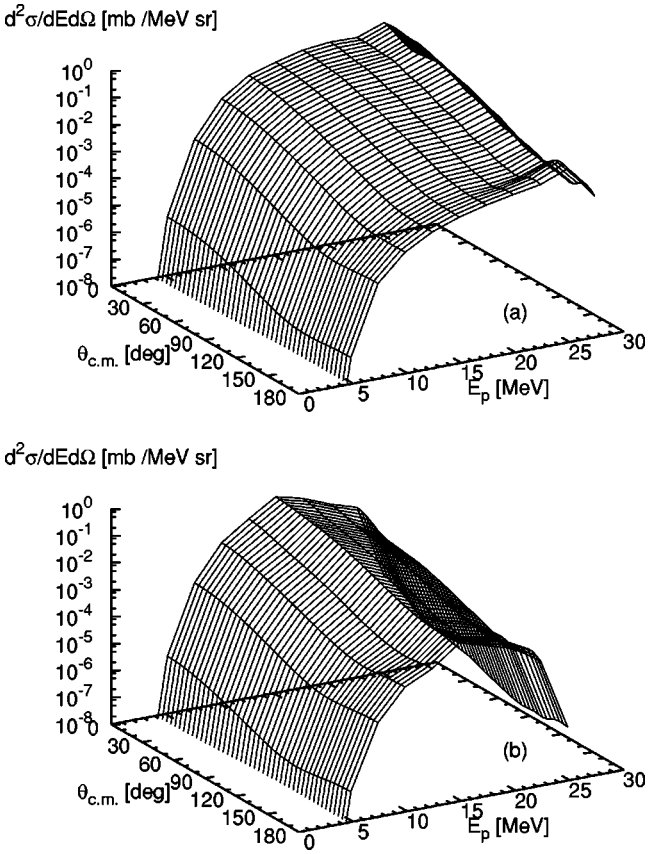

FIG. 12. 3D plot of the (a) one-step and (b) two-step cross sections for the reaction of ^{208}Pb(p,p') at $E_{\rm in}=30$ MeV.

We adopted the random-sampling method to average two-step DWBA cross sections. The number of sampled configuration should be large enough to get convergence of the averaged value. However, we could not reach the complete convergence because the two-step calculations take a great deal of computational time. We made several trials of the random-sampling technique, and estimated that the averaged cross sections have uncertainties of about 50% (this value is not 1σ but a rough estimation of the range of ambiguity). To avoid this relatively large ambiguity, a complete calculation should be made for all possible $2p$-$2h$ configurations in the M scheme. This may be possible for light nuclei such as ^{40}Ca.

An experimentally observed cross section is a sum of those cross sections (dashed line) together with the one-step cross section (dot-dashed line), which is shown by the thick solid line in Fig. 11. Contributions of higher steps can be neglected at this energy. The one-step cross section was calculated in a manner similar to the FKK calculations [25–27] except for a treatment of the level density, because the Ericson-Williams-type state densities [21–23] are often used for FKK-MSD calculations [7,25–27].

In the case of Fig. 11, the two-step cross section becomes larger than the one-step one, which seems to be peculiar if one compares it with published FKK analyses (see Refs. [25,26], for example). There are significant differences between FKK and our calculations. First, the FKK model employs an on-energy-shell approximation to calculate the Green's function, but we solve it exactly as in Eq. (7). Secondly, the FKK calculations contain a density of the $1p$-$1h$ state, while the NWY model uses a $2p$-$2h$ state density. In addition, state density formulas of the equidistant spacing model are often adopted in the FKK analyses, but those are different from our level density.

The relative strength of the two-step process to the one-step one is determined by the averaged DWBA cross section and the state density. The averaged one-step DWBA cross section is much larger than that for the two-step one; however, when those DWBA cross sections are multiplied by the state densities, the two-step cross section becomes comparable to that for the one-step one. In the case of $E_p=30$ MeV, the two-step contribution takes a maximum at $E_p'=15$ MeV. This will be shown later.

The ratio of the two-step cross sections to the one-step ones also depends on V_0, as the absolute value of the two-step cross section is proportional to V_0^4 while that for the one-step one is V_0^2. As the employed $V_0=30$ MeV is a tentative value, to determine the absolute two-step magnitude one needs to fit the calculated cross sections to experiments. Since we assumed a simple Yukawa interaction to calculate the second moments in Eq. (35), the level density $\rho_m(E)$ also depends on the V_0 value. At the low excitation energies where the partial level density rises rapidly with the excitation energy, a change in the saddle-point value σ_m by V_0 causes a large change in the level densities. However, the level density is quite insensitive to V_0 at high excitation en-

ergies, because the partial level densities are almost constant, as seen in Figs. 7 and 8, so that the effect of the energy shift by σ_m cannot be seen obviously. Therefore, one may be able to determine the V_0 value by fitting the absolute cross sections to the experimental data regardless of the level density calculation.

It is interesting to investigate an interference effect on the averaged two-step DWBA cross section. One can see in Fig. 4 that the effect appears in a certain $2p$-$2h$ configuration, but such interference is expected to disappear when one calculates an averaged cross section for a large number of configurations. We compared two cases. (a) All two-step cross sections were calculated with Eq. (22), and (b) Eq. (23) was used. These two cases yielded the same angular distribution but the absolute value was different. The difference is, however, about the same magnitude as the uncertainty of our calculations. Therefore, it is difficult to mention the effect of interference in the final result at this moment, and further study is needed.

The calculations described above were carried out for various outgoing proton energies to construct a double-differential cross section, and the result is shown in Figs. 12(a) and 12(b). The reaction is ^{208}Pb(p,p') with an incident proton energy of 30 MeV. The one-step cross sections are generally larger than the two-step ones except for $E_p'=15$ MeV, as is shown in Fig. 11. Below $E_p'=15$ MeV, the one-step and two-step cross sections show a similar tendency because of the Coulomb barrier. The one-step component dominates at the higher outgoing energies, so that the angle-energy-integrated cross section for the two-step component is about 20% of that for the one-step one in this calculation.

In this study, we have not compared our calculations with the experimental data, because the procedure adopted here is limited to doubly closed-shell nuclei. Such comparison is not difficult because our method can be extended to open-shell nuclei if a pairing correlation is introduced, and one can determine the strength of interaction, V_0. This should be done in future works.

IV. CONCLUSION

We described how two-step cross sections with the sudden approximation were calculated. The two-step process with the theory of Nishioka, Weidenmüller, and Yoshida is calculated as a microscopic two-step DWBA cross section which is averaged over the residual state. So the physical interpretation of the sudden approximation is quite straightforward.

Cross sections which excite a $2p$-$2h$ state were expressed in a J scheme, and the Yukawa-type interaction was assumed for the particle-hole pair creation. The Green's function appearing in the two-step calculation was represented in r space. An interference effect among the amplitudes for the different intermediate states was examined. A strong interference appeared for a certain configuration, and this was interpreted by the boson approximation.

The partial level densities for fixed J^π and exciton number were calculated with the model of Sato, Takahashi, and Yoshida [12]. The obtained ''true level densities'' were used for the calculation of ^{208}Pb(p,p') reaction cross sections. A random-sampling method was adopted for a cross-section average, and the averaged two-step cross sections were multiplied by the true level density to give a final double-differential cross section.

Our two-step calculations still contain relatively large uncertainties at this moment because of a problem in the cross-section averaging. However, it was shown that the two-step cross sections were almost in the same magnitude as the one-step ones below $E_p'=15$ MeV, when an incident proton energy was 30 MeV. Above the emission energy of 15 MeV, the one-step component dominates the two-step contribution.

ACKNOWLEDGMENTS

One of the authors (T.K.) is grateful to Professor M. Kawai and Professor Y. Watanabe at Kyushu University for valuable discussions. The author also thanks Dr. Hasegawa, Dr. Shibata, and Dr. Fukahori at Japanese Nuclear Data Center of Japan Atomic Energy Research Institute for supporting this work.

[1] E. Gadioli and P. E. Hodgson, *Pre-Equilibrium Nuclear Reactions* (Clarendon, Oxford, 1992).

[2] H. Feshbach, A. Kerman, and S. Koonin, Ann. Phys. (N.Y.) **125**, 429 (1980).

[3] T. Tamura, T. Udagawa, and H. Lenske, Phys. Rev. C **26**, 379 (1982).

[4] H. Nishioka, H. A. Weidenmüller, and S. Yoshida, Ann. Phys. (N.Y.) **183**, 166 (1988).

[5] A. J. Koning and J. M. Akkermans, Ann. Phys. (N.Y.) **208**, 216 (1991).

[6] M. B. Chadwick, F. S. Dietrich, A. K. Kerman, A. J. Koning, S. M. Grimes, M. Kawai, W. G. Love, M. Herman, F. Petrovich, G. Walker, Y. Watanabe, H. Wolter, M. Avrigeanu, E. Běták, S. Chiba, J. P. Delaroche, E. Gadioli, S. Hilaire, M. S. Hussein, T. Kawano, R. Lindsay, A. Marcinkowski, B. Marianśki, M. Mustafa, E. Ramström, G. Reffo, W. A. Richter, M. A. Ross, and S. Yoshida, Acta Phys. Slov. **49**, 365 (1999).

[7] A. Koning and J. M. Akkermans, Phys. Rev. C **47**, 724 (1993).

[8] T. Kawano and S. Yoshida, in *Proceedings of the 9th International Conference on Nuclear Reaction Mechanisms*, Varenna, Italy, 2000, edited by E. Gadioli (Ricerca Scientifica ed Educazione Permanente, Milano, 2000), Supplemento No. 115, p. 181.

[9] H. Lenske, H. H. Wolter, M. Herman, and G. Reffo, in *Proceedings of the International Conference on Nuclear Data for Science and Technology*, Trieste, Italy, 1997, edited by G. Reffo, A. Ventura, and C. Grandi (Italian Physical Society, Bologna, 1997), p. 231.

[10] E. Ramström, H. Lenske, and H. Wolter, in *Proceedings of the International Conference on Nuclear Data for Science and Technology* (Ref. [9]), p. 241.

[11] H. Nishioka, H. A. Weidenmüller, and S. Yoshida, Phys. Lett. B **203**, 1 (1988).

[12] K. Sato, Y. Takahashi, and S. Yoshida, Z. Phys. A **339**, 129 (1991).

[13] G. R. Satchler, Nucl. Phys. **55**, 1 (1964).
[14] N. Hashimoto and M. Kawai, Prog. Theor. Phys. **59**, 1245 (1978).
[15] N. Hashimoto, Prog. Theor. Phys. **59**, 1562 (1978).
[16] N. Austern, R. M. Drisko, E. Rost, and G. R. Satchler, Phys. Rev. **128**, 733 (1962).
[17] M. B. Johnson, L. W. Owen, and G. R. Satchler, Phys. Rev. **142**, 748 (1966).
[18] R. L. Walter and P. P. Guss, in *Proceedings of the International Conference on Nuclear Data for Basic and Applied Science*, Santa Fe, 1985, edited by P.G. Young, R.E. Brown, G.F. Auchampaugh, P.W. Lisowski, and L. Stewart (Gordon and Breach, New York, 1985), p. 1079; Radiat. Eff. **95**, 73 (1986).
[19] K. Sato and S. Yoshida, Z. Phys. A **327**, 421 (1987).
[20] T. Bengtsson and I. Ragnarsson, Nucl. Phys. **A436**, 14 (1985).
[21] E. Běták and J. Dobeš, Z. Phys. **A279**, 319 (1976).
[22] T. Ericson, Philos. Mag., Suppl. **9**, 425 (1960).
[23] F. C. Williams, Nucl. Phys. **A166**, 231 (1971).
[24] N. Yamamuro, Report No. JAERI-M 90-006, 1990.
[25] A. J. Koning and M. B. Chadwick, Phys. Rev. C **56**, 970 (1997).
[26] M. B. Chadwick and P. G. Young, Phys. Rev. C **47**, 2255 (1993).
[27] T. Kawano, T. Ohsawa, M. Baba, and T. Nakagawa, Phys. Rev. C **63**, 034601 (2001).